Effects of porosity on the elastic behaviour of CVI SiC/SiC composites at the scale of the tow: Representative Volume Element, Effective Behaviour and Stress Concentrations

L. Gélébart[1], C.Colin[1]

[1] *CEA Saclay, SRMA, BP49, 91191 cedex, Gif/Yvette, France*

KEYWORDS: SiC/SiC, porosity, periodic homogenization, representative volume element.

ABSTRACT

The purpose of this paper is to deal with the effect of the complex geometry of CVI composite's porosity on the elastic behaviour at the scale of the tow, which is an intermediate scale before the modelling of the woven composite. Microstructures are simulated and used in finite element calculations with periodic boundary conditions to determine both the effective behaviour and the local stress distribution. At first, the size of the Representative Volume Element (RVE) is discussed by comparing the behaviour of 5 simulated microstructures based on a random distribution of 150 fibres. It is evidenced that a domain of 150 fibres is not representative of the effective behaviour. This conclusion can be related to the complex geometry of the porosities with a strong heterogeneity of size and shape (some porosities are quite elongated). Then, the effective behaviour is studied from an average on the five microstructures. This behaviour exhibits a transverse isotropic symmetry with a strong anisotropy. In order to highlight the interest of this numerical approach, it is compared to a classical Mori-Tanaka approach assuming a circular cylindrical shape of the porosity. Finally, the effect of porosity is evaluated at the local scale. Porosity gives rise to a high level of stress heterogeneities that depends on the loading. These results (size of the RVE, anisotropy of the behaviour, stress concentrations) have to be taken into account when dealing with the further scale transition (modelling of the woven composite) and the initiation of damage.

1 INTRODUCTION

In the context of the development of future fission and fusion nuclear reactor, SiC/SiC composites are candidate for structural or functional applications at elevated temperature. A multi-scale approach is required to have a predictive modelling of their complex behaviour. The different scales of this approach are based on the observation of the composite: at the scale of the structure, the composite can be regarded as an homogeneous material; at the scale of the woven composite is only considered an assembly of woven tows (the constituents are the tows and the macro-porosity); at the scale of the tow, only the constituents of the tow (the fibres, the matrix, the interface and the porosity) are considered. The purpose of this paper focuses on the elastic behaviour of the composite at the scale of the tow (figure 1) in order to highlight the fact that the complex geometry of the porosity in CVI (Chemical Vapor Infiltration) composites plays a significant role on both the effective behaviour and the local stress distribution. A numerical procedure is developed to account for this complex geometry on the elastic behaviour. Moreover, its effect on the dimension of the Representative Volume Element is discussed. All the following results are fundamental results that have to be accounted for in the further modelling at the scale of the woven composite.

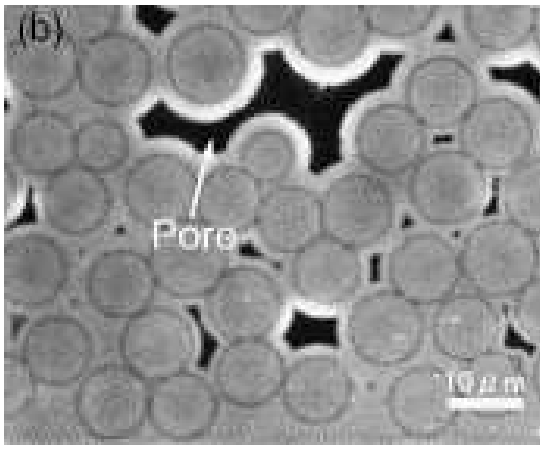

Figure 1: Typical microstructure of a CVI composite at the scale of the tow [1]

2 HOMOGENIZATION PROCEDURE

2.1 Generation of representative microstructures

The first step of homogenization procedures lies in a representation of the microstructures. In this paper, the microstructures are assumed to be invariant in the direction of the fibres and the cross section is obtained from a random distribution of fibres. The diameter of the fibres is assumed to be the same for all the fibres (7.5µm which corresponds to Tyranno SA3 fibres) and a usual volume fraction of fibres of 40% is used to generate a microstructure of 150 fibres randomly distributed in a square area of $129\times129\mu m^2$. Notice that the size of this area has been chosen large enough to be able to assume that the volume fraction of fibres is constant from one distribution to another. In order to discuss the representativity of these volume elements, five different distributions of fibres are used.
For CVI SiC/SiC composites, the process of SiC deposition on the fibres doesn't allow to fill completely the inter-fibres space so that a residual porosity appears within the tow (figure 1 [1]). To represent such microstructures, the infiltrated matrix is simulated by a layer of constant thickness of 3µm at the surface of the fibres (figure 2). The volume fractions of

residual porosity obtained for the 5 distributions of fibres are quite similar (6.8%, 7.2%, 7.4%, 7.5% and 7.5%) with a mean value of 7.3% which is in good agreement with microstructural observations [2]. The procedure to generate and to mesh such random microstructures has been developed with the free software *Salome* [3].

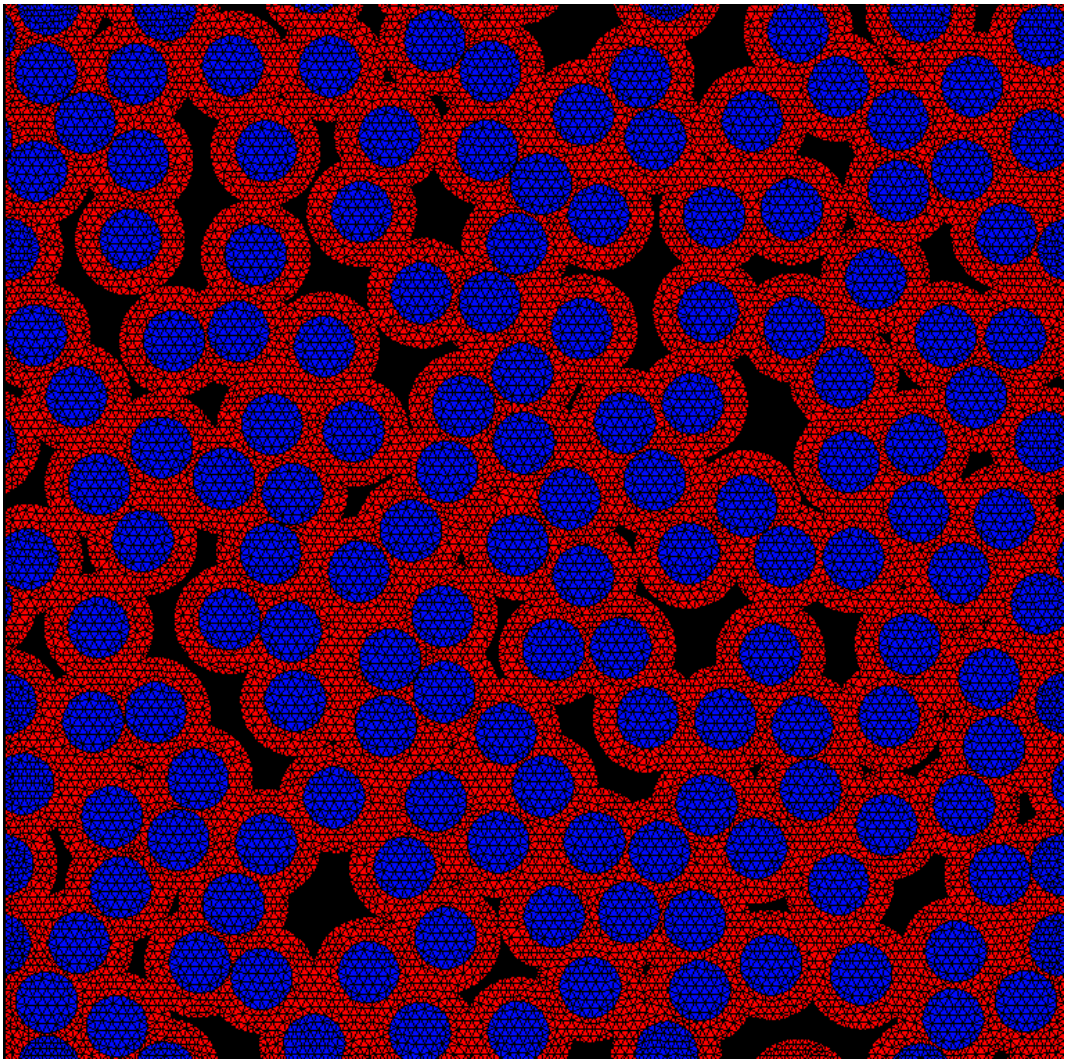

Figure 2: Simulated microstructure (due to the resolution of the picture, the mesh on the microstructure is hard to see)

2.2 Material parameters

The local anisotropy of the matrix, induced by the local crystallographic texture of the SiC deposition [4], is neglected compared to the effect of porosity. The matrix elastic behaviour is assumed to be isotropic with a Young modulus and a Poisson coefficient of 400GPa and 0.18, respectively.

Fibres candidate for nuclear applications are Hi-Nicalon S or Tyranno SA3 fibres. These fibres have a near-stoechiometric composition, a nanocrystallised microstructure and no crystallographic texture. Their elastic properties are close to the elastic properties of pure Beta-SiC. For Tyranno SA3, the Young modulus (measured at CEA [5]), is 389GPa and the Poisson coefficient is assumed to be 0.18.

2.3 Numerical homogenization

In order to solve the elastic problem of periodic homogenization with a finite element code (*CAST3M* [6]), the geometry of the microstructure described in section 2.1 (figure 2), defined in a parallelepiped volume, has been meshed using linear prismatic elements (6 nodes and 6 integration points), with one element in the thickness. The resulting mesh is periodic (i.e. each node on a surface has a corresponding node on the opposite surface). The set of differential equations used to solve this elastic problem are the classical volume equations for elasticity problems (local equilibrium, compatibility of the displacement field, elastic behaviour) added to periodic boundary conditions with a stress piloting. The description of these boundary conditions introduced for that purpose in *CAST3M* [6] is not detailed in this paper. A first property associated to these boundary conditions is that the mean stress on the whole microstructure V is equal to the applied stress tensor $\underline{\underline{\Sigma}}$ given as an entry of the elastic problem (equation 1). The second property [7] is that the mean strain can evaluated, as a post-treatment, from the displacements of corresponding points (M, M^*) in opposite surfaces of the microstructure's boundary (Equation 2 - figure 3). This last property is important for porous microstructures because the local strain is not defined within the porosity so that the mean strain on the whole microstructure (including porosity) can't be evaluated from the spatial integration of the local strain.

Equation 1 $$<\underline{\underline{\sigma}}>_V = \underline{\underline{\Sigma}}$$

Equation 2 $$\underline{u}(M) - \underline{u}(M^*) = <\underline{\underline{\varepsilon}}>_V . \underline{MM^*}$$

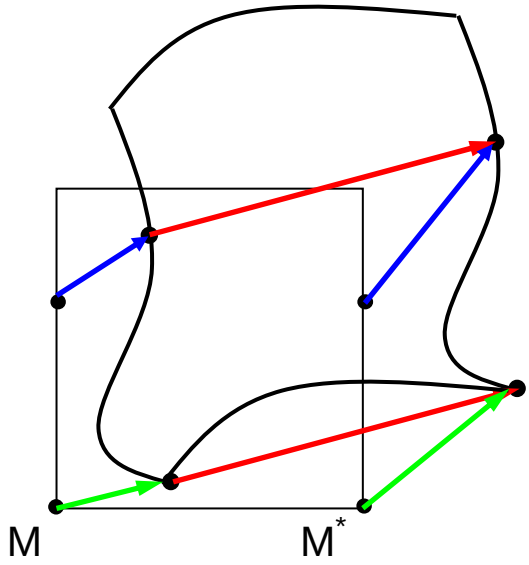

Figure 3: Schematic visualization of the periodic boundary condition: the red vector is constant for all corresponding points in opposite surfaces (then $<\underline{\underline{\varepsilon}}>_V$ can be deduced from equation 2).

As a result, the stiffness tensor of the i-th microstructure $\widetilde{K}^i$ (equation 3) can be fully determined from six different simulations performed with six different applied stresses $\underline{\underline{\Sigma}}$.

Equation 3 $$<\underline{\underline{\sigma}}>_V = \widetilde{K}^i :: <\varepsilon>_V$$

3 REPRESENTATIVITY OF THE VOLUME ELEMENT

3.1 Evaluation of the effective behaviour

At first, the average stiffness tensor $\overline{K}$ is evaluated from the average value on the 5 stiffness tensors $\widetilde{K}^i$. From the description of the microstructure, the effective behaviour is expected to satisfy a transverse isotropic symmetry. The effective stiffness tensor $\widetilde{K}$ (Equation 4) is deduced from the adjustment of the coefficients of $\overline{K}$ in order to satisfy strictly the symmetry conditions. However, as shown in equations 5 (a-d), the differences between the coefficients of $\overline{K}$ and $\widetilde{K}$ reveal that this adjustment is very slight.

Equation 4

$$\widetilde{K} = \begin{pmatrix} 251.2 & 55.5 & 55.2 & 0 & 0 & 0 \\ 55.5 & 251.2 & 55.2 & 0 & 0 & 0 \\ 55.2 & 55.2 & 386.4 & 0 & 0 & 0 \\ 0 & 0 & 0 & 195.7 & 0 & 0 \\ 0 & 0 & 0 & 0 & 241.9 & 0 \\ 0 & 0 & 0 & 0 & 0 & 241.9 \end{pmatrix}$$

Equation 5-a $$\left|\overline{K_{11}} - \overline{K_{22}}\right| / \widetilde{K}_{11} = 2.2\%$$

Equation 5-b $$\left|\overline{K_{13}} - \overline{K_{23}}\right| / \widetilde{K}_{13} = 1.8\%$$

Equation 5-c $$\left|\overline{K_{55}} - \overline{K_{66}}\right| / \widetilde{K}_{55} = 1.3\%$$

Equation 5-d $$\left|\overline{K_{11}} - \left(\overline{K_{44}} + \overline{K_{12}}\right)\right| / \widetilde{K}_{11} = 0.7\%$$

3.2 Fluctuation of the stiffness tensor

The comparison between the different stiffness tensors $\widetilde{K}_i$ is summarized in equation 6. It can be seen that the difference from one microstructure to another can be higher than 25%. Moreover, the fluctuations from the transverse isotropy are summarized in equations 7, the discrepancy on the symmetry conditions can be as much as 18.7%. From these two results, it can be concluded that a single domain of 150 fibres (which represents in our case, 129*129µm^2) can not be considered as "representative" from the point of view of the elastic effective behaviour. This point will have to be considered when dealing with the further scale transition: at the scale of the woven composite, can the tow be considered as homogeneous?

Equation 6

$$\left(\max_{i \neq j} \left(\widetilde{K}^i_{mn} - \widetilde{K}^j_{mn} \right) \Big/ \widetilde{K}_{mn} \right) = \begin{pmatrix} 15.6 & 14.8 & 14.4 & & & \\ 14.8 & 29.6 & 25 & & & \\ 14.4 & 25 & 1.4 & & & \\ & & & 12.8 & & \\ & & & & 17.1 & \\ & & & & & 9.7 \end{pmatrix}_{\%}$$

Equation 7-a $$\max_i \left| \widetilde{K}_{11}^i - \widetilde{K}_{22}^i \right| / \widetilde{K}_{11} = 18.7\%$$

Equation 7-b $$\max_i \left| \widetilde{K}_{13}^i - \widetilde{K}_{23}^i \right| / \widetilde{K}_{13} = 15.3\%$$

Equation 7-c $$\max_i \left| \widetilde{K}_{55}^i - \widetilde{K}_{66}^i \right| / \widetilde{K}_{55} = 11.4\%$$

Equation 7-d $$\max_i \left| \widetilde{K}_{11}^i - (\widetilde{K}_{44}^i + \widetilde{K}_{12}^i) \right| / \widetilde{K}_{11} = 4.2\%$$

3.3 Discussion on the "mechanical" Representative Volume Element (RVE)

Several arguments can explain that these quite important domains (150 fibres) with a representative volume fraction of porosity (~7.3%) are not representative from the point of view of the effective mechanical behaviour. The first point is that the size of the "mechanical RVE" (the RVE associated to the effective mechanical behaviour) increases when the elastic contrast between the constitutive phases of a material increases. As porosity can be considered as an elastic phase with a null stiffness, the elastic contrast is infinite so that the size and the shape of the porosity plays a significant role on the size of the RVE. Moreover, when looking at figures 1 and 2, if the number of fibres is 150, the number of porosities is almost divided by 3 compared to the number of fibres. Finally it can be seen that the shape and the size of the porosities are very heterogeneous and that the larger porosities have a typical size of 3 or 4 fibres diameters. All these arguments can be raised to explain an important size of the mechanical RVE.

The results presented in the following sections, 4 and 5, are dealing with the effective behaviour $\widetilde{K}$ deduced from an average on the 5 stiffness tensors $\widetilde{K}_i$ (see section 3.1).

4 EFFECT OF POROSITY ON THE EFFECTIVE BEHAVIOUR

In order to emphasize the relevance of this numerical approach, a classical analytical Mori-Tanaka model (see equations in [8]) is used assuming a simplified geometry of the porosity (circular cylinders with a volume fraction of 7.3%). In this calculation, the elastic heterogeneity between matrix and fibres (400GPa and 389GPa) is reasonably neglected (the Young modulus is assumed to be equal to 395GPa for both the matrix and the fibres). The effective stiffness tensor obtained with the Mori-Tanaka model $\widetilde{K}^{MT}$ is given in equation 8. To visualize the anisotropy of the behaviour and the difference between the two approaches, the evolution of the apparent elastic modulus as a function of the angle between the fibres and the tensile test direction is represented on figure 4.

Equation 8
$$\widetilde{K}^{MT} = \begin{pmatrix} 350.6 & 84.6 & 78.3 & 0 & 0 & 0 \\ 84.6 & 350.6 & 78.3 & 0 & 0 & 0 \\ 78.3 & 78.3 & 394.4 & 0 & 0 & 0 \\ 0 & 0 & 0 & 298.7 & 0 & 0 \\ 0 & 0 & 0 & 0 & 302.9 & 0 \\ 0 & 0 & 0 & 0 & 0 & 302.9 \end{pmatrix}$$

When the tensile test direction is parallel to the direction of the fibres, the two models are consistent and the apparent Young modulus can be obtained with a classical mixture rule for a parallel assembly. In this direction, there is no effect of the geometry of the porosity.

On the contrary, when the tensile test direction is perpendicular to the direction of the fibres, the Mori-Tanaka model is much stiffer the periodic homogenization model. This difference reveals that the complex shape of the porosity has to be taken into account through a numerical approach to obtain a good description of the elastic anisotropy of the composite.

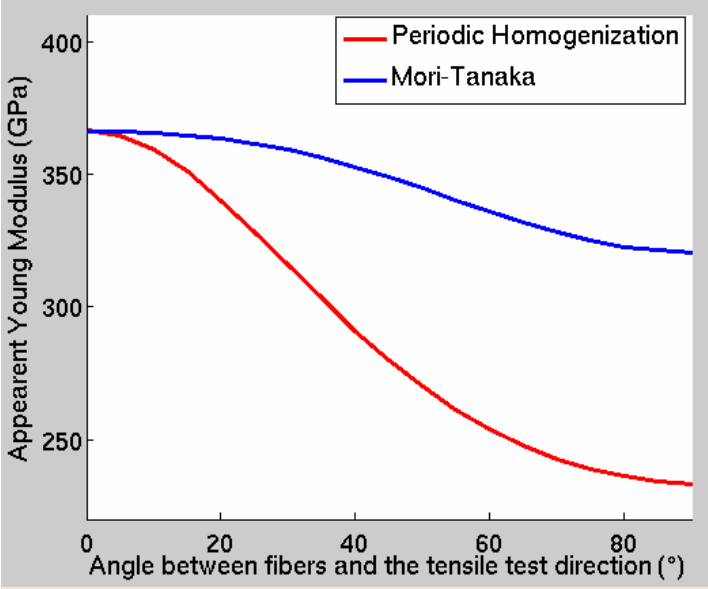

Figure 4: Evolution of the apparent elastic modulus as a function of the tensile test direction

5 EFFECT OF POROSITY ON THE STRESS DISTRIBUTION

The numerical approach can also be used to evaluate the full distribution of the local stresses which can't be evaluated from analytical models.
For a tensile test direction parallel to the direction of the fibres, the microstructure can be regarded as a parallel assembly (with identical Poisson coefficients). Consequently, the stress field is uniaxial and homogeneous within the fibres and the matrix. When the angle between the tensile test direction and the fibres direction increases, the heterogeneity of the axial stress increases (figures 5 and 6). The development of such heterogeneities is characterized by the development of a second peak associated to stress discharges within the material and to the development of a wide queue of the distribution associated to the development of stress concentrations within the material. The comparison between figures 5 and 6 reveals that the stress concentrations are much higher within the matrix than within the fibres. As stress concentrations and discharges are arising from the porosities (figure 7), the matrix is more affected by these stress heterogeneities. Finally, the stress distributions (figures 5 and 6) can be related to the observation of the axial stress field for a macroscopic tensile test of 1GPa perpendicular to the fibres direction. The stress field can be schematized by blue and green bands parallel to the tensile test direction that corresponds to the two peaks observed on the stress distributions (figures 5 and 6), and by a few red regions that correspond to the wide queue of the distributions on figures 5 and 6 (i.e. the high stress concentrations).

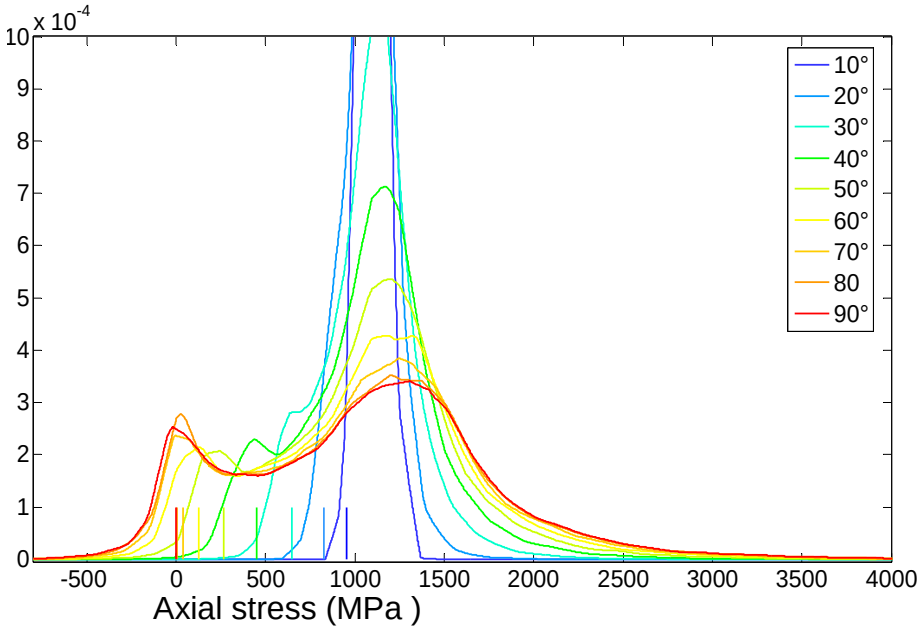

Figure 5: Distributions of the axial stress field within the matrix for different orientation of a 1GPa macroscopic tensile test direction (with respect to the fibres direction).

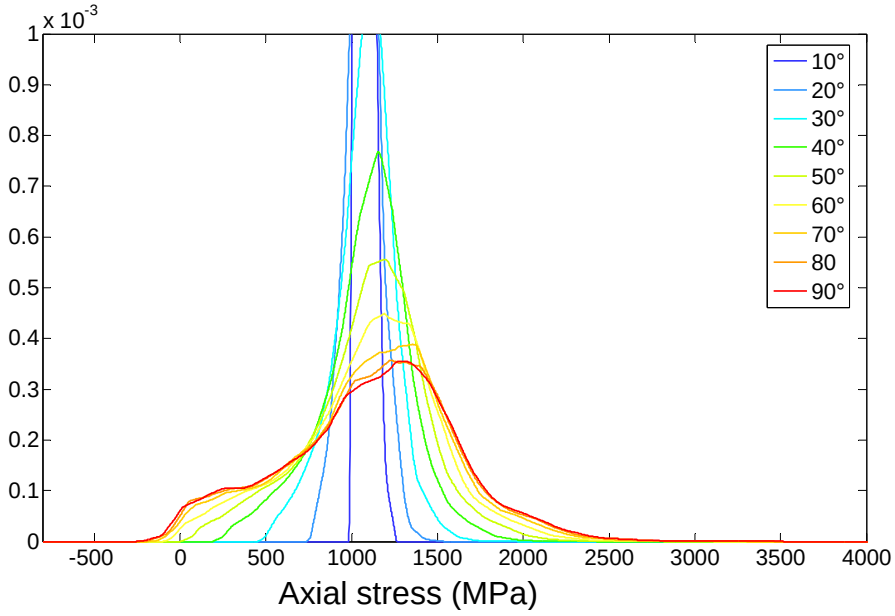

Figure 6: Distribution of the axial stress field within the fibres for different orientations of a 1GPa macroscopic tensile test direction with respect to the fibres direction.

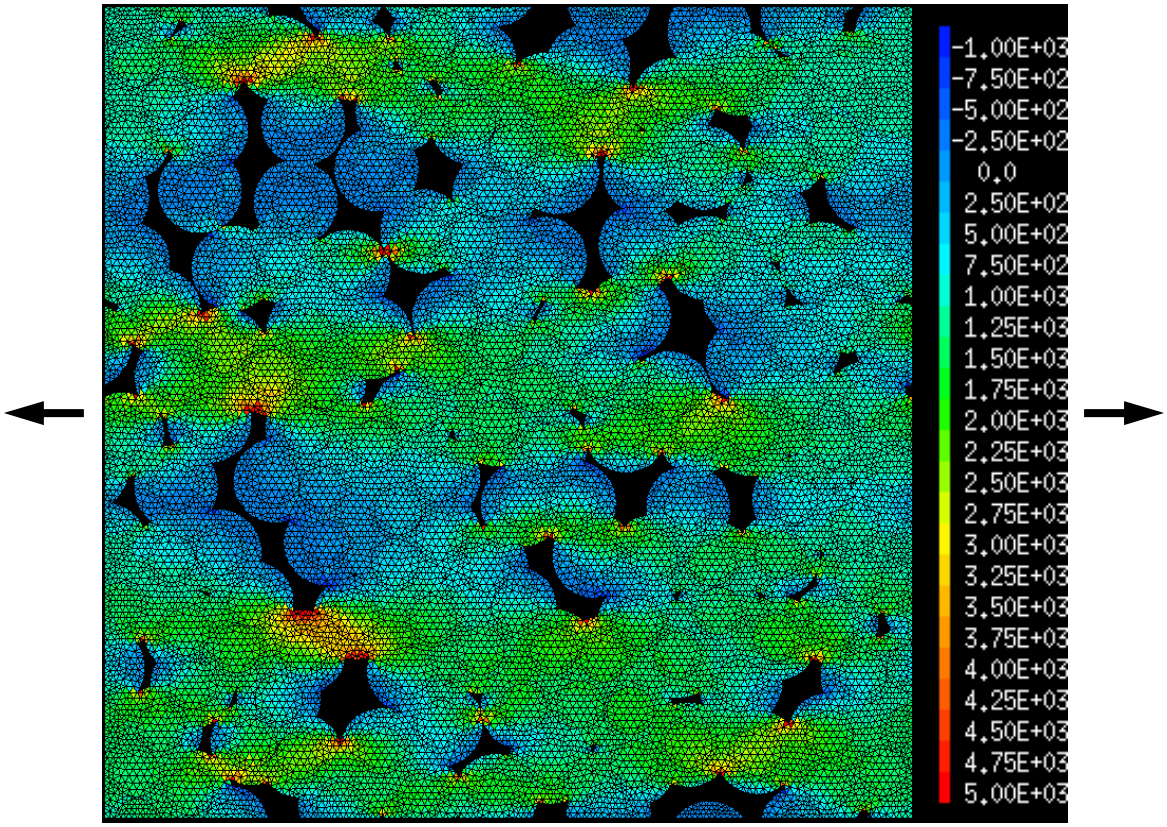

Figure 7: Axial stress field for a macroscopic tensile test (1GPa) in the transverse direction.

6 CONCLUSIONS

In order to evaluate the effect of the complex geometry of the porosity on the elastic behaviour of CVI SiC/SiC composites at the scale of the tow, a numerical procedure has been developed. The first step of this procedure consists in simulating representative microstructures. The method to generate such microstructures is inspired from the deposition of SiC matrix on the fibres in the CVI process. The second step consists in the development of a periodic homogenization procedure within the finite element code CAST3M[6].

From 5 simulated microstructures, with 150 fibres in the microstructures, it has been shown that this size of microstructure is not large enough to be considered as representative.

However, the effective stiffness tensor was deduced from the average stiffness tensors on these 5 microstructures. This behaviour exhibit a strong anisotropic behaviour. The comparison to a classical Mori-Tanaka approach with circular cylinder porosity has revealed that the complex geometry of the porosity plays a significant role and has to be taken into account. Finally, such a numerical approach was able to evaluate the effect of the porosity on the stress heterogeneity within the CVI composite. It has been shown that the porosity gives rise to stress discharges within the material but also to a high level of stress concentrations.

These results on the size of the Representative Volume Element, on the anisotropy of the elastic behaviour of the tow and on the stress concentrations at the local scale will have to be taken into account when dealing with the modelling of the woven composite and the initiation of damage.

REFERENCES

[1] Fabrication of SiC fiber reinforced SiC composite by chemical vapor infiltration for excellent mechanical properties, Igawa N., Taguchi T., Nozawa T., Snead L.L., Hinoki T., McLaughlin J.C., Katoh Y., Jitsukawa S., Kohyama A., Journal of Physics and Chemistry, Vol.66, pp551-554, 2005

[2] Approches statistiques-probabilistes du comportement mécanique des composites à matrice céramique, Calard V , PhD Thesis, University of Bordeaux 1, 1998

[3] http://salome-plateforme.org

[4] EBSD investigation of SiC for HTR fuel particles, D. Helary, O. Dugne, X. Bourrat, P.H. Jouneau and F. Cellier, Journal of Nuclear Materials, Vol.350(3), pp 332-335, 2006

[5] Caractérisations mécaniques et microstructurales de fibres de SiC pour le développement de nouveaux matériaux des centrales nucléaires de 4ème génération, Pierquet L., Gélébart L., Cozzika T., Doriot S., Pelé J., Onimus F., Hamon D., Gosmain L., Martin H., Bonnaillie P., CEA Internal Report, DMN/SRMA/LC2M/2006-2791/A, 2006

[6] http://www-cast3m.cea.fr

[7] Determination of the representative volume element for random composites: statistical and numerical approach. Kanit T., Forest S., Galliet I., Mounoury V., Jeulin D., International Journal of Solids and Structures, Vol.40, pp3647-3679, 2003

[8] Effects of void geometry on elastic properties of unidirectionnal fibre reinforced composites, Huang H., Taljera R., Composites Science and Technology, Vol.65, pp1964-1981, 2005